optica

Subwavelength nanocavity for flexible structural transmissive color generation with a wide viewing angle

Kyu-Tae Lee,[1] Ji-Yun Jang,[2] Sang Jin Park,[2] Ujwal Kumar Thakur,[2] Chengang Ji,[1] L. Jay Guo,[1] and Hui Joon Park[2,3,*]

[1]Department of Electrical Engineering and Computer Science, The University of Michigan, Ann Arbor, Michigan 48109, USA
[2]Department of Energy Systems Research, Ajou University, Suwon 16499, South Korea
[3]Department of Electrical and Computer Engineering, Ajou University, Suwon 16499, South Korea
*Corresponding author: huijoon@ajou.ac.kr

Received 22 August 2016; revised 29 October 2016; accepted 7 November 2016 (Doc. ID 274293); published 12 December 2016

We present a high angular tolerant structural coloration based on strong interference effects in a nanocavity patterned at a subwavelength scale on a flexible substrate. The structural colors, fabricated over a large area by nanoimprint lithography, feature a non-iridescent performance over a wide angle of incidence up to 60°, which is of great importance to various applications, such as imaging sensors and colored display systems. In addition to the non-iridescence, the transmissive colors of the proposed structure, simply consisting of triple layers, can be tuned with ease by altering a duty cycle of nanostructures, thus enabling the creation of individual RGB colors in a pixel unit via a facile one-step approach. Moreover, it is confirmed that their performances remain unchanged to the 10 mm bending radius condition, and the encapsulation effects of a polymer material on their optical properties are investigated for practical usage. The presented strategy could provide a new avenue for achieving improved efficiency and desired functionality, thereby opening the door to many potential applications, including anti-counterfeit tagging, imaging sensor systems, and color e-paper displays.

OCIS codes: (230.5750) Resonators; (330.1690) Color; (050.2230) Fabry-Perot; (310.6628) Subwavelength structures, nanostructures.

https://doi.org/10.1364/OPTICA.3.001489

1. INTRODUCTION

As an alternative to the present chemical-based color filter systems, a structural color filter scheme, which exploits a physical interaction of light with nano- and micro-structures (e.g., photonic and plasmonic resonances), has been widely investigated due to its potential advantages, such as ultra-compactness, long-standing stability, and simple manufacturability [1–9]. In addition, a concept of photon recycling for better energy efficiency could be realized with structural color filter systems, as they only use a certain spectral region of visible light for color generation while strongly reflecting the complementary spectrum that could be potentially harvested by other structures to produce different colors. For this purpose, various structural configurations, based on guided-mode resonances (GMRs) [10–14], Fabry–Pérot resonances [15–23], surface plasmon resonances (SPRs) [24–34], photonic crystals [35,36], and localized resonances [37,38] have been extensively studied.

Particularly with the growing popularity of high-definition devices, the ability to create color pixels beyond the diffraction limit has been another key feature of the structural color filter system. Therefore, in recent years, with the rapid developments of large-scale nanofabrication techniques such as nanoimprint lithography (NIL) [39–43], roll-to-roll processing [44,45], colloidal self-assembly [26,46], and laser interference lithography [32], a substantial amount of attention has been given to the various nanostructure-based color filtering systems, which could provide unique possibilities for enabling color printing with subdiffraction resolution. However, there have been great difficulties in retaining optical resonances at the same wavelength over a wide angular range and simultaneously creating vivid full colors in a pixel unit through a one-step facile pattering process. This is mainly because the majority of periodic nanostructure-based color filtering schemes have been based on the excitation of SPR or GMR for color generation, inherently causing angle-sensitive performance due to momentum matching conditions. To mitigate such angular-dependent properties, a variety of schemes incorporating a highly absorbing medium-based thin-film nanocavity, high refractive index materials, or phase compensating overlay have been conceived [16,36,47,48]; however, the cavity layer thickness should be changed to tune the colors, which requires three individual lithographic processes to demonstrate red, green, and blue (RGB) colors in a pixel unit. In addition, the metallic subwavelength structures could alleviate the angular dependence by light funneling, as was suggested, but the complex fabrication processes for deep nanogroove arrays limit their application to flexible and wearable displays over large areas [38]. Consequently, there is a strong need to develop a new strategy that can address the aforementioned

Corrected 31 January 2017

challenges altogether by providing new functionalities, such as angle-insensitivity, one-step simple processibility, and flexibility.

Here, we demonstrate a flexible, non-iridescent transmissive structural color printing scheme employing strong optical interference behaviors in a lossy medium-based nanocavity patterned at the subwavelength scale over large areas (2 cm × 2 cm) via NIL. Transmissive colors created by the proposed structures are less sensitive to incident angles, meaning the spectral response of the structures remains nearly similar for wide angles of incidence up to 60°. Additionally, resonant wavelengths are shifted by controlling the width of the nanogratings rather than the layer thickness of the nanostructures, therefore requiring only one lithographic step to pattern each individual pixel, which is distinctly different from the traditional colorant pigment-based counterparts, where three accurately aligned lithographic patterning steps should be involved. Lastly, the optical responses of the proposed structural color filter against bending deformation were investigated, and the effects of a thin polymeric encapsulation layer on their performance are explored.

2. METHODS

A. Device Fabrication

The large-area amorphous silicon (a-Si) nanogratings were fabricated by NIL-based processes. NIL was performed in an EITRE-8 naonoimprinter (OBDUCAT) using a silicon dioxide (SiO_2) mold on a poly(methyl methacrylate) (PMMA) resist spin-cast on the SiO_2(25 nm)/silver (Ag)(20 nm)/copper (Cu)(1 nm) substrates, at a pressure of 35 bar and a temperature of 140°C, for 5 min. SiO_2, Ag, and Cu were sequentially deposited on the transparent substrate using an E-beam evaporator. After cooling and demolding, chromium (Cr) was selectively deposited on each sidewall of the imprinted grating structures by angled deposition. The Cr deposited on the resist patterns induced the undercut structures during O_2 reactive ion etching (RIE), facilitating the lift-off process. O_2 RIE (10 sccm O_2, 40 mTorr chamber pressure, and 40 W bias power), deposition of a-Si using the e-beam evaporator, and the lift-off process completed the fabrication of a-Si nanograting structures on a substrate. As for the flexible color filter, polyethylene terephthalate (PET) was utilized as a substrate instead of glass. For encapsulation, a PMMA solution was spin-cast on the devices, and the concentration of the solution and rpm of the spin-casting were adjusted to control its thickness.

B. Optical Characterization and Simulation

Transmission spectra at normal incidence and angle-resolved transmission spectra were measured using a visible spectrometer (V-770 UV-Visible-Near Infrared Spectrophotometer, JASCO). Commercial COMSOL Multiphysics software, based on the finite-element method, was carried out to explore spectral curves of transmittance at normal incidence, angle-resolved transmission spectra, and normalized electric field intensity distribution. The refractive indices of Ag, a-Si, and SiO_2 were measured using a spectroscopic ellipsometer (Elli-SE, Ellipso Technology Co.). A net phase shift as a function of an incident angle at a resonance wavelength for the RGB structural colors was calculated by the effective medium theory.

3. RESULTS AND DISCUSSION

Figure 1(a) depicts the schematic representation of the proposed nanocavity-based angle-insensitive structural colors, composed of

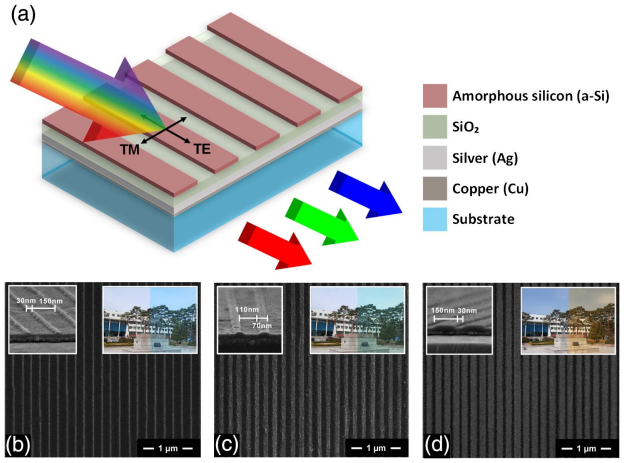

Fig. 1. (a) Schematic representation of the proposed subwavelength nanocavity-based transmissive structural color filters, composed of a-Si nanogratings on top of SiO_2 (25 nm) and an optically transparent metallic substrate (Ag = 20 nm). Top-view SEM images of (b) blue (B), (c) green (G), and (d) red (R) of fabricated structural color filters. Insets show angle-view SEM images and photographs of the fabricated samples where a background monument can be seen through the samples with the RGB colors.

ultrathin semiconductor gratings patterned at the subwavelength scale on top of an optically transparent metallic film with a spacer layer. Recently, a scheme exploiting the strong optical resonance effects in the ultrathin semiconductor-based nanocavity, where a non-trivial phase shift (i.e., not 0 or π) occurs when reflecting from a semiconductor-metal interface due to a large imaginary part of the complex refractive index of the semiconductor material (i.e., optical absorption loss), which has been demonstrated in a large number of applications, including structural coloration, decorative solar cells, and thermal emitters [18,19,21,22,49–51]. This behavior is obviously different from traditional Fabry–Pérot resonance, which generally appears in a quarter-wavelength-thick cavity layer. One of the key characteristics of such unconventional Fabry–Pérot cavity resonances is the capability of achieving a wide-angle performance that is attributed to a negligible phase accumulated in passing through the ultrathin semiconductor layer. In order to control the angular dependence and color purity at the same time, it is necessary for the semiconductor material to have optical absorptions that are neither too strong nor too weak. For example, low-bandgap semiconductors such as germanium (Ge) have a large absorption coefficient across the entire visible spectrum, causing poor color purity, while wide-bandgap semiconductors such as SiO_2 have a negligible absorption loss in the visible range, making it difficult to create the strong optical resonance in the ultrathin cavity thickness regime. According to this design rationale, a-Si is selected as a highly absorbing medium, and Ag is chosen as the metallic reflector, as its absorption loss is the lowest while providing the highest reflectivity in the visible range among the noble metals. In this device structure, the period of the nanograting (P) and the semiconductor thickness (t) are fixed at 180 and 10 nm, respectively. The thicknesses of the intermediate spacer layer (SiO_2) and the bottom metallic film (Ag) are 25 and 20 nm, respectively. Increasing the width (W) of the nanogratings allows an effective refractive index of the nanocavity medium to be increased, therefore leading to a resonance shifted toward the longer

wavelength range. For blue, green, and red (B, G, R) color generation, 30, 70, and 150 nm grating widths are used. Note that the proposed structure is designed to be one-dimensionally patterned, enabling the colors to be produced only under transverse-electric (TE) polarized light illumination (i.e., the electric field of the incident light oscillates in the direction parallel to the nanogratings), so the SPR, whose resonance is highly sensitive to the angle of incidence, propagating at the metal-dielectric interface cannot be excited. The Ag and SiO_2 layers were deposited using an electron-beam evaporator, sequentially, and a-Si nanogratings was prepared on the SiO_2 layer using a NIL-based simple lift-off process for large-area pattern formation. Before Ag film formation, a 1 nm Cu seed layer was additionally deposited using an e-beam evaporator to improve the uniformity of the following Ag film [52]. The details on the device fabrication are given in the Experimental Methods section. Figures 1(b)–1(d) provide top-view scanning electron microscope (SEM) images of the fabricated RGB structural colors, all of which exhibit well-defined top semiconductor grating patterns. The inset images show angled-view SEM images and photographs of the fabricated samples.

Figure 2(a) presents simulated spectral transmittance curves of the proposed structural color filters under TE polarized light illumination at a normal incident angle, which were carried out using commercial finite element method COMSOL Multiphysics

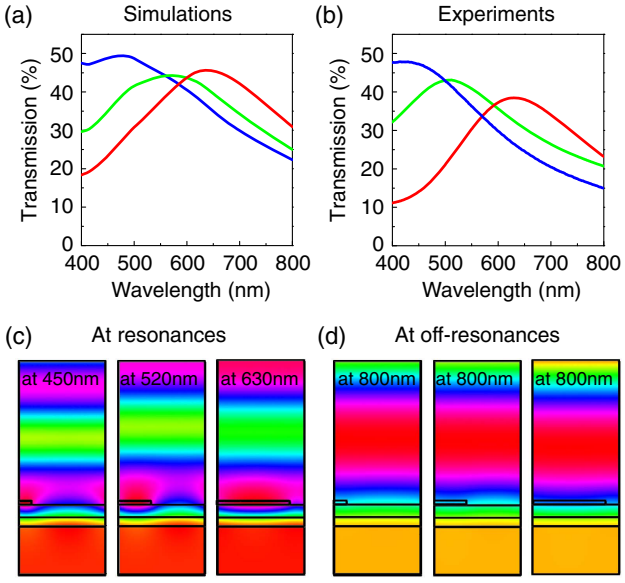

Fig. 2. (a) Simulated and (b) measured transmission spectra at normal incidence. The measured profiles show slightly blue-shifted resonances (B: 450 nm, G: 520 nm, R: 630 nm) as compared to those obtained from the simulation (B: 475 nm, G: 560 nm, R: 640 nm), which could be due to the oxidation of ultrathin a-Si nanogratings and dimensional deviations during the fabrication of the structural color filters. For creating individual RGB colors in a pixel unit via a one-step fabrication method, a period ($P = 180$ nm) and a thickness ($t = 10$ nm) are fixed. The transmissive colors are tuned by changing the width (W) of the subwavelength gratings: B ($W = 30$ nm), G ($W = 70$ nm), and R ($W = 150$ nm). Distributions of normalized z component of electric field into a device structure at (c) resonances and at (d) off-resonances (800 nm). It is obvious that the electric field intensity is strongly confined in the a-Si subwavelength gratings presenting the fundamental resonance mode at the resonant wavelength, while the electric field is reflected at the off-resonant wavelength. The red and blue colors represent the high and low intensities of the electric field, respectively.

software. In the simulation, the refractive indices of a-Si, Ag, and SiO_2 were measured using a spectroscopic ellipsometer (Elli-SE, Ellipso Technology Co.), as shown in Fig. S1, Supplement 1, and 1.45 was used as the refractive index of the glass substrate. As shown in Fig. 2(b), those calculated transmittance spectra exhibited a good match with the measured spectra. The simulated (measured) data show transmission resonances appearing at 640 (630), 560 (520), and 475 (450) nm for red, green, and blue (R, G, B) color generation, and the slight difference between the simulated and the measured resonances may be attributed to the oxidation of the top ultrathin a-Si gratings. Such oxidation led to the reduced index of refraction of the a-Si material and hence, the resonance could shift toward shorter wavelength ranges. Additionally, dimensional deviations (e.g., the thickness of each layer and the widths of the gratings) and a surface roughness, induced during the device fabrication, could be other causes of their discrepancy. It is important to note that the color purity can be improved by placing an additional thin Ag layer on top of the nanogratings [18]. As mentioned earlier, RGB colors can be easily tuned by controlling the width of the semiconductor nanogratings (30, 70, and 150 nm for B, G, and R colors, respectively) with the fixed thickness and the period of the gratings (10 and 180 nm, respectively), which is appealing as a facile one-step fabrication process for the color pixel fabrication.

It is important to note that inserting the buffer SiO_2 spacer layer between the semiconductor gratings and the bottom metallic reflector can improve the light–matter interaction and therefore the transmission efficiency, as it prevents incident light from being further penetrated into the metallic mirror by compensating the phase mismatch so that the ohmic loss in the metal reflector could be mitigated [53,54]. The effect of the phase compensation layer on the transmission efficiency and the resonance behaviors with and without SiO_2 are shown in Fig. S2 of Supplement 1, and about 5% enhanced transmission is achieved after introducing the spacer layer between the lossy medium-based nanogratings and the metallic layer. Such improved transmission efficiency is more definite when the resonance is created at the shorter wavelength where the metallic reflector has a higher absorption loss compared to the longer wavelength range. Moreover, the red-shifted resonance is observed, and this is due to the increased cavity layer thickness with the spacer layer. We note that with increasing the thickness of the Ag layer in the structure, it is observed: (1) the resonance gets sharp (i.e., high Q-factor resonance) with reduced transmission efficiency due to the increased reflections, and (2) the resonance is shifted toward shorter wavelengths due to different phase shifts occurring upon reflection at the semiconductor-metal interface (see Fig. S3, Supplement 1).

Due to the extensibility of the NIL-based printing process and the angle insensitivity of the designed color filter, which will be discussed in more detail later, the proposed structures can be easily created on a flexible substrate with a negligible change in the resulting color appearance, thus potentially offering the intriguing possibility of numerous applications, such as flexible electronics, wearable displays, and color e-paper technologies. For achieving a flexible functionality, the proposed structural color filters were fabricated on a PET substrate. In order to be applied in practical applications, it is quite important to retain a high transmission efficiency at a fixed resonance position with decreasing a radius of curvature. Figures 3(a) and 3(b) present a measured maximum value of transmission efficiency and the resonance position for the individual RGB structural

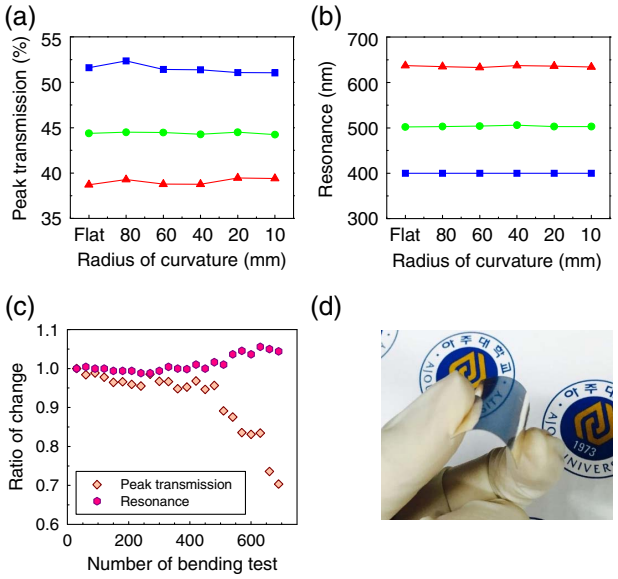

Fig. 3. (a) A peak of the transmission efficiency and (b) a position of the resonance as a function of the radius of curvature. Red-, green-, and blue-colored symbols represent the data from the red, green, and blue color filters. (c) Ratio of change of transmission efficiency and resonance wavelength according to the number of bending tests. (d) A photograph of the fabricated blue color filter on a flexible substrate.

colors, both of which show insensitivity with respect to the radius of curvature, indicating no color change when the entire structure is bent on the plastic substrate. We could not find any specific differences between the performance variation from bending in parallel and that in the perpendicular direction to a-Si nanogratings. Even at the minimum radius of curvature condition (10 mm), the maximum change of the period of a-Si nanogratings, which can affect the resonance, is just around a nanometer range, and the strain values of a-Si, SiO_2 and Ag layers are lower than their failure strains; therefore, consistent optical performances without mechanical failure could be achieved. Figure S4 of Supplement 1 shows that the period change of the a-Si nanograting from 180 to 190 nm does not provide any spectrum difference in the RGB structural colors. Though the variation of optical properties by bending was investigated only down to the 10 mm radius of curvature condition due to the limitation of the bending property of the PET substrate, it is expected that a smaller bending radius condition without a performance change would be possible with other flexible substrate having better bendability. A more detailed mechanics analysis is underway. Additionally, the durability of the color filters was confirmed by continuous bending tests, and it was shown that the optical performances of the color filters were retained even after about five hundred bending tests [Fig. 3(c)].

An optical image of the fabricated flexible blue color filter is shown in Fig. 3(d). It is obvious that there is no color difference over the entire surface of the plastic substrate, which is greatly desired in a broad range of color printing applications. A simple device structure where the subwavelength gratings are ultrathin-patterned on top of the two thin films provides distinct advantages over the previously reported works that involve complex and expensive fabrication techniques.

The mechanism of the resonance could be further explored by normalized electric field intensity distributions at the resonant wavelength and at the off-resonant wavelength, numerically analyzed for the RGB colored samples, as presented in Figs. 2(c) and 2(d), respectively. As depicted in Fig. 2(c), the electric field is strongly concentrated into the semiconductor nanogratings where the fundamental Fabry–Pérot resonant mode appears at the resonance leading to light transmission, while the electric field is reflected back toward the incident medium at the off-resonance, as exhibited in Fig. 2(d). Note that the red and blue colors in the electric field distribution represent the high and low intensities, respectively. The semiconductor subwavelength gratings can be regarded as a thin-film layer with the effective refractive index, which is determined by the filling ratio of the semiconductor gratings and air, and the effective index of refraction for TE polarization (n_{TE}) can be calculated by Eq. (1) [55,56],

$$n_{TE} = \sqrt{\epsilon_1 f + \epsilon_2 (1-f)} \sqrt{1 + \frac{\pi^2}{3}(\epsilon_1 f + \epsilon_2 (1-f)) \left(\frac{f(1-f)P}{\lambda}\right)^2 \left(\frac{\epsilon_1 - \epsilon_2}{\epsilon_1 f + \epsilon_2 (1-f)}\right)}, \quad (1)$$

where f, P, ϵ_1, and ϵ_2 are a duty cycle, the periodicity of the nanogratings, the permittivity of the semiconductor material, and that of air, respectively. The effective refractive indices of the one-dimensional (1D) grating structures are obtained from a linear and inverse linear mixing of the permittivity of the constitutive materials (i.e., a-Si and air) by a volume fraction ratio for TE and transverse magnetic (TM) polarizations, respectively. It was reported that the effective medium theory is still valid for the case where the thickness of the gratings is ultrathin as compared to the wavelength of incident light [57]. The effective complex refractive index of the subwavelength gratings of the individual RGB colors and the corresponding transmission spectra, calculated by the effective medium theory, are described in Fig. S5, Supplement 1. As the linewidth of the nanogratings increases to create the resonance at the longer wavelength, the value of the complex refractive index increases due to the large proportion of the semiconductor. The transmission profiles, predicted by the effective medium theory [Fig. S5(b), Supplement 1], are in great agreement with the numerically simulated results in Fig. 2(a).

The calculated and measured spectral transmittance curves under TM-polarized light at normal incidence are also provided in Figs. S6(a) and S6(b) of Supplement 1. For TM polarization where an oscillating direction of the electric field is perpendicular to the subwavelength gratings, the effective refractive index of the cavity calculated by the effective medium theory is relatively smaller than that for TE polarization, as can be seen from Fig. S6(c), Supplement 1. In particular, the imaginary part of the effective refractive indices for the blue- and green-colored structures is nearly negligible (i.e., the cavity medium becomes transparent), indicating that strong optical interference effects in the ultrathin semiconductor layer cannot occur. As a result, any resonance (i.e., transmission peak) associated with such strong interferences is not observed in either the simulated and measured transmission spectra [see Figs. S6(a) and S6(b), Supplement 1] for the blue and green colors. Instead, SPR propagating at the interface between SiO_2 and Ag can be excited at the 500 nm wavelength, which can be found in the field distribution into the device structures, as displayed in Fig. S6(d), Supplement 1. For

the blue color, the efficiency of coupling incident light into the SPR is not high as compared to other colors due to the narrower nanogratings. To avoid an SPR-driven incident-angle-sensitive spectral response, which dramatically limits numerous applications, our structural color filters are designed to operate only under TE-polarized light illumination.

Next, a dependence of the resonance on the incident angle, which is of critical importance to various applications, is explored. The optical responses of many previous works that rely on a grating coupling mechanism to couple an incident light wave to either the plasmonic or the photonic resonant mode are easily affected by the change of incident angle due to the momentum matching condition, thereby imposing practical limitations. In contrast, our structural color filter designs are based on the strong interference behaviors in the ultrathin absorptive medium-based nanocavity patterned at a subwavelength scale with a fixed period, featuring an angle-insensitive performance. This is because the resonance condition is predominantly fulfilled by the phase shift occurring upon the reflection at the metal-semiconductor interface rather than the phase shift accumulation in the propagation. The non-trivial reflection phase shift also compensates the insignificant propagation phase shift, thus leading to the flat dispersion characteristics. Note that the top semiconductor nanogratings are 1D patterned and only work for TE polarization so the intrinsic angle-dependent property of the plasmonic resonance that can be excited by TM polarization is not involved.

Figures 4(a)–4(f) represent the simulated and measured angular responses in the transmission of the proposed structural color filters for TE polarization from normal incidence to 60°. As can be seen from those figures, the resonant wavelength, where a transmission peak is represented by a bright color, remains almost constant over a wide angular range up to 60°. Such an angle-invariant feature is enabled by suppressing the phase shift accumulated during the propagation through the cavity medium having an ultrathin

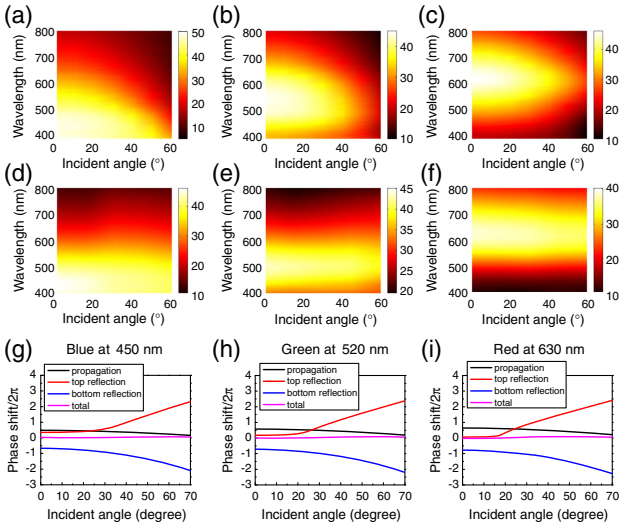

Fig. 4. (a)–(c) Simulated and (d)–(f) measured angle-resolved transmission spectra of the proposed structural color filters where the resonance (i.e., bright color) in the dispersion curve is insensitive with respect to angles of incidence from 0° to 60°. A net phase change (magenta) that involves propagation (black) and reflection phase shifts (red and blue) as a function of the incident angles at the resonance conditions of (g) B, (h) G, and (i) R colors, calculated by effective medium theory, exhibiting a flat-band characteristic.

thickness compared to the light wavelength. Figures 4(g)–4(i) provide a net phase shift, encompassing the two reflection phase shifts and the propagation phase shift, as a function of the incident angle ranging from 0° to 60° at the resonance conditions of the individual RGB colors, calculated by the effective medium theory. It is apparent that the change in the propagation phase shift (black color) is trivial and is canceled out by the non-trivial reflection phase shifts (red and blue colors), thereby allowing the total phase shift to be invariant over a wide range of incident angles.

As previously pointed out, it is fairly easy for the a-Si nanogratings to be oxidized because the thickness is only 10 nm, which can cause a color shift and a performance degradation over time. In order to resolve this challenge, the entire structures are encapsulated by a thin polymer material, PMMA, to prevent the ultrathin a-Si nanogratings from being oxidized. As the thickness of the encapsulation layer affects the optical spectral response and therefore the resulting colors, it is important to optimize the thickness of the protective layer. Figure 5(a) describes the calculated spectral transmittance curves of the green-colored filters according to the thickness of the polymer encapsulation layer, and they show a good match with the measured transmission data in Fig. 5(b). As compared to the resonance without the PMMA protective layer (black), it is clear that the resonance gets sharp when the encapsulation film has the proper thickness, resulting in the improved color purity. This could be ascribed to the

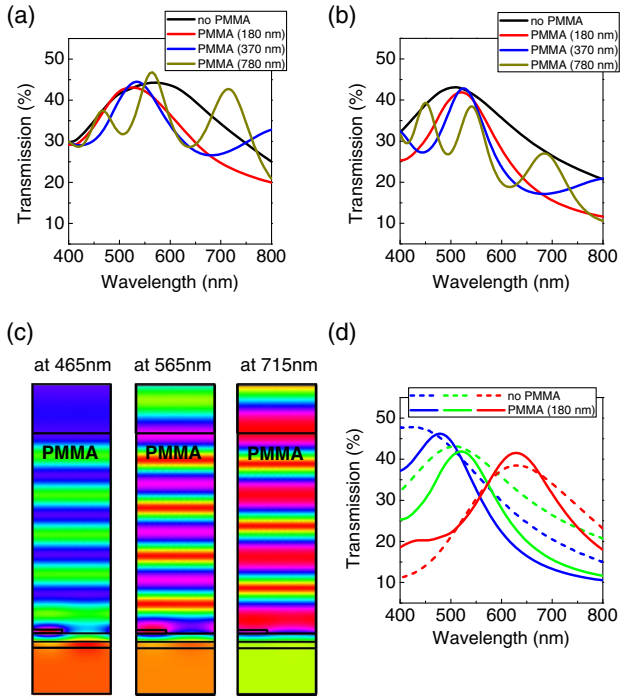

Fig. 5. (a) Simulated and (b) measured transmission spectra of green color filter at normal incidence with and without a polymer encapsulation layer atop the structure. (c) Normalized z component of electric field distributions of the structure, where the green color ($W = 70$ nm) is created, with a 780-nm-thick top encapsulation layer at the 465, 565, and 715 nm wavelengths, each of which corresponds to the resonance (i.e., peak positions in the transmission) as shown in (a). (d) Measured transmission spectra of the structural color filters without (dotted lines) and with (solid lines) a polymer encapsulation layer (180 nm), the latter of which shows a sharp resonance (i.e., improved Q-factor) leading to high color purity.

better impedance matching, allowing a large amount of incident light to be constructively interfered at the resonance. Such a sharp resonant behavior, however, could be affected by increasing the encapsulation film thickness. As can be seen from the transmission spectrum obtained with the 780-nm-thick PMMA layer, a single resonance is split into three different resonant modes, where an additional Fabry–Pérot resonance in the PMMA film becomes dominant upon increasing the thickness of the protective layer. Figure 5(c) shows the normalized intensity distribution of electric field in the green-colored structural color filter, coated by the 780-nm-thick PMMA encapsulation layer, at the peak positions of the transmission spectrum. At the 465 nm wavelength, the field is mainly concentrated into the a-Si subwavelength gratings, indicating the Fabry–Pérot resonance in the ultrathin patterned nanocavity layer, whereas the field is strongly confined in the encapsulation layer at the 715 nm wavelength, to which the PMMA thickness is comparable. Interestingly, it is observed that a hybrid resonance mode, where the field in the nanogratings couples with that in the encapsulation PMMA film, exists at an intermediate wavelength (565 nm). It was found that the optimal thickness of the PMMA encapsulation layer was ~180 nm, as depicted in Fig. 5(d), showing that the transmission profiles with the encapsulation (solid lines) have a sharper resonance than those without the encapsulation layer (dotted lines).

4. CONCLUSION

In summary, we have demonstrated flexible and ultrathin (<60 nm) structural color filters creating wide-angle transmission colors exploiting strong optical interference behaviors in the absorptive medium-based nanocavity where the top semiconductor film was patterned at the subwavelength scale. The individual RGB color filters, which could be extended to the flexible plastic substrate via NIL, were insensitive to angles of incidence up to 60° for TE polarization, which was attributed to the fact that the optical phase was mainly accumulated at the interfaces, leading to the insignificant propagation phase. It was also demonstrated that only one patterning process was needed to generate a unit pixel having three individual RGB colors, which was markedly different from a variety of approaches described in the previous reports as well as conventional chemical pigment-based color filters, where three precisely aligned independent patterning steps are required in order to create the color pixels, thereby potentially expanding the range of possible applications. To avoid the oxidation of the ultrathin semiconductor nanogratings, the structural color filters were coated by a thin polymer material that not only functioned as a protective layer but improved the color purity due to the better impedance matching. Furthermore, the optical characteristics of the structural colors when the devices are bent on the flexible substrate were investigated. The described approach represents an important step toward the realization of various applications, such as flexible electronics, e-paper technologies, decorations, and photosensors.

Funding. Korea Evaluation Institute of Industrial Technology (KEIT) (10051565); Ministry of Trade, Industry and Energy (MOTIE); Korea Display Research Corporation (KDRC); Korea Institute of Energy Technology Evaluation and Planning (KETEP) (2015 4010 200820); Basic Science Research Program; National Research Foundation of Korea (NRF) (2014R1A1A2056403).

Acknowledgment. K. T. L. and J. Y. J. contributed equally to this work.

See Supplement 1 for supporting content.

REFERENCES

1. F.-J. Ko and H.-P. D. Shieh, "High-efficiency micro-optical color filter for liquid-crystal projection system applications," Appl. Opt. **39**, 1159–1163 (2000).
2. P. B. Catrysse, W. Suh, S. Fan, and M. Peeters, "One-mode model for patterned metal layers inside integrated color pixels," Opt. Lett. **29**, 974–976 (2004).
3. Y. Kanamori, M. Shimono, and K. Hane, "Fabrication of transmission color filters using silicon subwavelength gratings on quartz substrates," IEEE Photon. Technol. Lett. **18**, 2126–2128 (2006).
4. H. J. Park, T. Xu, J. Y. Lee, A. Ledbetter, and L. J. Guo, "Photonic color filters integrated with organic solar cells for energy harvesting," ACS Nano **5**, 7055–7060 (2011).
5. J. Y. Lee, K.-T. Lee, S. Seo, and L. J. Guo, "Decorative power generating panels creating angle insensitive transmissive colors," Sci. Rep. **4**, 4192 (2014).
6. K.-T. Lee, M. Fukuda, S. Joglekar, and L. J. Guo, "Colored, see-through perovskite solar cells employing an optical cavity," J. Mater. Chem. C **3**, 5377–5382 (2015).
7. V. Steenhoff, M. Theuring, M. Vehse, K. von Maydell, and C. Agert, "Ultrathin resonant-cavity-enhanced solar cells with amorphous germanium absorbers," Adv. Opt. Mater. **3**, 182–186 (2015).
8. R. W. Sabnis, "Color filter technology for liquid crystal displays," Displays **20**, 119–129 (1999).
9. K.-T. Lee, J.-Y. Jang, S. J. Park, C. Ji, S.-M. Yang, L. J. Guo, and H. J. Park, "Angle-insensitive and CMOS-compatible subwavelength color printing," Adv. Opt. Mater. **4**, 1696 (2016).
10. M. J. Uddin and R. Magnusson, "Highly efficient color filter array using resonant Si_3N_4 gratings," Opt. Express **21**, 12495–12506 (2013).
11. V. Raj Shrestha, S.-S. Lee, E.-S. Kim, and D.-Y. Choi, "Polarization-tuned dynamic color filters incorporating a dielectric-loaded aluminum nanowire array," Sci. Rep. **5**, 12450 (2015).
12. Y.-T. Yoon, H.-S. Lee, S.-S. Lee, S. H. Kim, J.-D. Park, and K.-D. Lee, "Color filter incorporating a subwavelength patterned grating in poly silicon," Opt. Express **16**, 2374–2380 (2008).
13. M. J. Uddin, T. Khaleque, and R. Magnusson, "Guided-mode resonant polarization-controlled tunable color filters," Opt. Express **22**, 12307–12315 (2014).
14. D. B. Mazulquim, K. J. Lee, J. W. Yoon, L. V. Muniz, B.-H. V. Borges, L. G. Neto, and R. Magnusson, "Efficient band-pass color filters enabled by resonant modes and plasmons near the Rayleigh anomaly," Opt. Express **22**, 30843–30851 (2014).
15. K.-T. Lee, S. Seo, and L. J. Guo, "High-color-purity subtractive color filters with a wide viewing angle based on plasmonic perfect absorbers," Adv. Opt. Mater. **3**, 347–352 (2015).
16. C.-S. Park, V. R. Shrestha, S.-S. Lee, and D.-Y. Choi, "Trans-reflective color filters based on a phase compensated etalon enabling adjustable color saturation," Sci. Rep. **6**, 25496 (2016).
17. K. Mao, W. Shen, C. Yang, X. Fang, W. Yuan, Y. Zhang, and X. Liu, "Angle insensitive color filters in transmission covering the visible region," Sci. Rep. **6**, 19289 (2016).
18. K.-T. Lee, S. Seo, J. Y. Lee, and L. J. Guo, "Strong resonance effect in a lossy medium-based optical cavity for angle robust spectrum filters," Adv. Mater. **26**, 6324–6328 (2014).
19. K.-T. Lee, S. Seo, J. Yong Lee, and L. Jay Guo, "Ultrathin metal-semiconductor-metal resonator for angle invariant visible band transmission filters," Appl. Phys. Lett. **104**, 231112 (2014).
20. C. Yang, W. Shen, Y. Zhang, K. Li, X. Fang, X. Zhang, and X. Liu, "Compact multilayer film structure for angle insensitive color filtering," Sci. Rep. **5**, 9285 (2015).
21. M. A. Kats, R. Blanchard, P. Genevet, and F. Capasso, "Nanometre optical coatings based on strong interference effects in highly absorbing media," Nat. Mater. **12**, 20–24 (2013).
22. M. A. Kats, S. J. Byrnes, R. Blanchard, M. Kolle, P. Genevet, J. Aizenberg, and F. Capasso, "Enhancement of absorption and color con-

trast in ultra-thin highly absorbing optical coatings," Appl. Phys. Lett. **103**, 101104 (2013).
23. J. Guo, C. M. Huard, Y. Yang, Y. J. Shin, K.-T. Lee, and L. J. Guo, "ITO-free, compact, color liquid crystal devices using integrated structural color filters and graphene electrodes," Adv. Opt. Mater. **2**, 435–441 (2014).
24. T. Xu, Y.-K. Wu, X. Luo, and L. J. Guo, "Plasmonic nanoresonators for high-resolution colour filtering and spectral imaging," Nat. Commun. **1**, 59 (2010).
25. F. Cheng, J. Gao, T. S. Luk, and X. Yang, "Structural color printing based on plasmonic metasurfaces of perfect light absorption," Sci. Rep. **5**, 11045 (2015).
26. L. Wang, R. J. H. Ng, S. Safari Dinachali, M. Jalali, Y. Yu, and J. K. W. Yang, "Large area plasmonic color palettes with expanded gamut using colloidal self-assembly," ACS Photon. **3**, 627–633 (2016).
27. F. Cheng, X. Yang, D. Rosenmann, L. Stan, D. Czaplewski, and J. Gao, "Enhanced structural color generation in aluminum metamaterials coated with a thin polymer layer," Opt. Express **23**, 25329 (2015).
28. J. Olson, A. Manjavacas, T. Basu, D. Huang, A. E. Schlather, B. Zheng, N. J. Halas, P. Nordlander, and S. Link, "High chromaticity aluminum plasmonic pixels for active liquid crystal displays," ACS Nano **10**, 1108–1117 (2016).
29. B. Y. Zheng, Y. Wang, P. Nordlander, and N. J. Halas, "Color-selective and CMOS-compatible photodetection based on aluminum plasmonics," Adv. Mater. **26**, 6318–6323 (2014).
30. F. Cheng, J. Gao, L. Stan, D. Rosenmann, D. Czaplewski, and X. Yang, "Aluminum plasmonic metamaterials for structural color printing," Opt. Express **23**, 14552 (2015).
31. B. Ai, Y. Yu, H. Möhwald, and G. Zhang, "Responsive monochromatic color display based on nanovolcano arrays," Adv. Opt. Mater. **1**, 724–731 (2013).
32. Y. S. Do, J. H. Park, B. Y. Hwang, S.-M. Lee, B.-K. Ju, and K. C. Choi, "Plasmonic color filter and its fabrication for large-area applications," Adv. Opt. Mater. **1**, 133–138 (2013).
33. D. Franklin, Y. Chen, A. Vazquez-Guardado, S. Modak, J. Boroumand, D. Xu, S.-T. Wu, and D. Chanda, "Polarization-independent actively tunable colour generation on imprinted plasmonic surfaces," Nat. Commun. **6**, 7337 (2015).
34. H. Yun, S.-Y. Lee, K. Hong, J. Yeom, and B. Lee, "Plasmonic cavity-apertures as dynamic pixels for the simultaneous control of colour and intensity," Nat. Commun. **6**, 7133 (2015).
35. O. Berger, E. Yoskovitz, L. Adler-Abramovich, and E. Gazit, "Spectral transition in bio-inspired self-assembled peptide nucleic acid photonic crystals," Adv. Mater. **28**, 2195–2200 (2016).
36. K.-T. Lee, C. Ji, D. Banerjee, and L. J. Guo, "Angular- and polarization-independent structural colors based on 1D photonic crystals," Laser Photon. Rev. **9**, 354–362 (2015).
37. R. Yu, P. Mazumder, N. F. Borrelli, A. Carrilero, D. S. Ghosh, R. A. Maniyara, D. Baker, F. J. García de Abajo, and V. Pruneri, "Structural coloring of glass using dewetted nanoparticles and ultrathin films of metals," ACS Photon. **3**, 1194–1201 (2016).
38. Y.-K. R. Wu, A. E. Hollowell, C. Zhang, and L. J. Guo, "Angle-insensitive structural colours based on metallic nanocavities and coloured pixels beyond the diffraction limit," Sci. Rep. **3**, 1194 (2013).
39. L. M. Cox, J. P. Killgore, Z. Li, Z. Zhang, D. C. Hurley, J. Xiao, and Y. Ding, "Morphing metal-polymer Janus particles," Adv. Mater. **26**, 899–904 (2014).
40. L. M. Cox, Z. Li, N. Sowan, D. Nair, J. Xiao, C. N. Bowman, and Y. Ding, "Reconfigurable surface patterns on covalent adaptive network polymers using nanoimprint lithography," Polymer **55**, 5933–5937 (2014).
41. S. H. Maruf, Z. Li, J. A. Yoshimura, J. Xiao, A. R. Greenberg, and Y. Ding, "Influence of nanoimprint lithography on membrane structure and performance," Polymer **69**, 129–137 (2015).
42. L. M. Cox, J. P. Killgore, Z. Li, R. Long, A. W. Sanders, J. Xiao, and Y. Ding, "Influences of substrate adhesion and particle size on the shape memory effect of polystyrene particles," Langmuir **32**, 3691–3698 (2016).
43. E.-H. Cho, H.-S. Kim, B.-H. Cheong, P. Oleg, W. Xianyua, J.-S. Sohn, D.-J. Ma, H.-Y. Choi, N.-C. Park, and Y.-P. Park, "Two-dimensional photonic crystal color filter development," Opt. Express **17**, 8621 (2009).
44. S. H. Ahn and L. J. Guo, "High-speed roll-to-roll nanoimprint lithography on flexible plastic substrates," Adv. Mater. **20**, 2044–2049 (2008).
45. J. G. Ok, Y. J. Shin, H. J. Park, and L. J. Guo, "A step toward next-generation nanoimprint lithography: extending productivity and applicability," Appl. Phys. A **121**, 343–356 (2015).
46. M. Xiao, Y. Li, M. C. Allen, D. D. Deheyn, X. Yue, J. Zhao, N. C. Gianneschi, M. D. Shawkey, and A. Dhinojwala, "Bio-inspired structural colors produced via self-assembly of synthetic melanin nanoparticles," ACS Nano **9**, 5454–5460 (2015).
47. C.-S. Park, V. R. Shrestha, S.-S. Lee, E.-S. Kim, and D.-Y. Choi, "Omnidirectional color filters capitalizing on a nano-resonator of Ag-TiO_2-Ag integrated with a phase compensating dielectric overlay," Sci. Rep. **5**, 8467 (2015).
48. V. R. Shrestha, S.-S. Lee, E.-S. Kim, and D.-Y. Choi, "Non-iridescent transmissive structural color filter featuring highly efficient transmission and high excitation purity," Sci. Rep. **4**, 4921 (2014).
49. M. A. Kats, D. Sharma, J. Lin, P. Genevet, R. Blanchard, Z. Yang, M. M. Qazilbash, D. N. Basov, S. Ramanathan, and F. Capasso, "Ultra-thin perfect absorber employing a tunable phase change material," Appl. Phys. Lett. **101**, 221101 (2012).
50. K.-T. Lee, J. Y. Lee, S. Seo, and L. Guo, "Colored ultrathin hybrid photovoltaics with high quantum efficiency," Light: Sci. Appl. **3**, e215 (2014).
51. L. Kyu-Tae, L. Jae Yong, S. Sungyong, and L. J. Guo, "Microcavity-integrated colored semitransparent hybrid photovoltaics with improved efficiency and color purity," IEEE J. Photovolt. **5**, 1654–1658 (2015).
52. N. Formica, D. S. Ghosh, A. Carrilero, T. L. Chen, R. E. Simpson, and V. Pruneri, "Ultrastable and atomically smooth ultrathin silver films grown on a copper seed layer," ACS Appl. Mater. Interfaces **5**, 3048–3053 (2013).
53. H. Song, L. Guo, Z. Liu, K. Liu, X. Zeng, D. Ji, N. Zhang, H. Hu, S. Jiang, and Q. Gan, "Nanocavity enhancement for ultra-thin film optical absorber," Adv. Mater. **26**, 2737–2743 (2014).
54. H. Song, S. Jiang, D. Ji, X. Zeng, N. Zhang, K. Liu, C. Wang, Y. Xu, and Q. Gan, "Nanocavity absorption enhancement for two-dimensional material monolayer systems," Opt. Express **23**, 7120–7130 (2015).
55. R. Haïdar, G. Vincent, N. Guérineau, S. Collin, S. Velghe, and J. Primot, "Wollaston prism-like devices based on blazed dielectric subwavelength gratings," Opt. Express **13**, 9941–9953 (2005).
56. R. Bräuer and O. Bryngdahl, "Design of antireflection gratings with approximate and rigorous methods," Appl. Opt. **33**, 7875–7882 (1994).
57. B. C. P. Sturmberg, T. K. Chong, D.-Y. Choi, T. P. White, L. C. Botten, K. B. Dossou, C. G. Poulton, K. R. Catchpole, R. C. McPhedran, and C. Martijn de Sterke, "Total absorption of visible light in ultrathin weakly absorbing semiconductor gratings," Optica **3**, 556–562 (2016).